Earth and Planetary Science Letters 612 (2023) 118150

Contents lists available at ScienceDirect

Earth and Planetary Science Letters

journal homepage: www.elsevier.com/locate/epsl

Barium isotope signatures of barite–fluid ion exchange in Equatorial Pacific sediments

J.T. Middleton [a,b,c,*], A. Paytan [d], M. Auro [a,b], M.A. Saito [b], T.J. Horner [a,b]

[a] NIRVANA Labs, Woods Hole Oceanographic Institution, Woods Hole, MA, USA
[b] Department of Marine Chemistry & Geochemistry, Woods Hole Oceanographic Institution, Woods Hole, MA, USA
[c] MIT–WHOI Joint Program in Oceanography, Woods Hole, MA, USA
[d] Institute of Marine Science, University of California, Santa Cruz, CA, USA

ARTICLE INFO

Article history:
Received 21 November 2022
Received in revised form 27 March 2023
Accepted 28 March 2023
Available online xxxx
Editor: L. Coogan

Keywords:
diagenesis
porewater
paleoceanography
geochemistry

ABSTRACT

The isotope composition of barium (Ba) in the mineral barite ($BaSO_4$) is emerging as a powerful tracer of the pelagic Ba, carbon, and sulfur cycles. However, it is critical to identify and constrain processes that may alter the primary isotope composition of Ba, δ^{138}Ba, in $BaSO_4$, particularly during early diagenesis. To this end, we analyzed the Ba isotope composition of porewaters and co-located $BaSO_4$ in sediments from the Equatorial Pacific and performed a series of laboratory experiments with these same $BaSO_4$ to assess rates of Ba isotope alteration. We find that sedimentary $BaSO_4$ exhibit Ba isotope compositions $\approx$+0.1‰ and are offset by ≈ -0.16‰ relative to ambient porewaters. Experiments using isotope-labeled seawater show extensive and rapid transfer of Ba ions between the solid and fluid phase through coupled $BaSO_4$ dissolution-precipitation, even at chemical equilibrium. Using published values for Ba isotope fractionation during $BaSO_4$ precipitation and dissolution, we calculate that co-located $BaSO_4$ and porewaters should exhibit Ba isotope offset of -0.17‰ at isotopic equilibrium, similar to the offsets observed in Equatorial Pacific sediments. Altogether, the field data, laboratory experiments, and calculations indicate that ion exchange occurs in Equatorial Pacific sediments and that this process also drives the observed Ba isotope offsets between pelagic $BaSO_4$ and porewaters. This finding implies that ion exchange may alter the isotope composition of Ba in sedimentary $BaSO_4$, though the degree of alteration will depend on the proportion of Ba held in the solid phase. More broadly, this study provides an example of how ion-exchange-mediated processes are widespread in marine geochemistry and that these processes likely affect other metals and minerals beyond Ba and $BaSO_4$.

1. Introduction

Barite ($BaSO_4$) in pelagic sediments has long been used as an archive of seawater isotope compositions of sulfur, oxygen, strontium, and calcium, as well as the impacts of microbial sulfur cycling on seawater sulfur isotopes (Paytan et al., 2004, 2002; Turchyn and Schrag, 2006, 2004). In addition to its chemistry, the accumulation rate of $BaSO_4$ in pelagic sediments offers a record of marine export productivity over centennial to millennial timescales (Dymond et al., 1992; Paytan and Griffith, 2007). Recent advances in Ba stable isotope geochemistry have added a new dimension for studying Ba cycling, including refinement of the global marine Ba cycle (Cao et al., 2020; Crockford et al., 2019; Horner et al., 2015; Hsieh et al., 2021; Hsieh and Henderson, 2017), tracking Ba sources to aquatic and marine environments (Bridgestock et al., 2021; Cao et al., 2021, 2020; Guo et al., 2020; Hodgskiss et al., 2019), tracing deep water mass mixing (Bates et al., 2017; Geyman et al., 2019; Hemsing et al., 2018; Horner et al., 2017), and reconstructions of Ba cycling from the rock record (Bridgestock et al., 2019; Yu et al., 2022; Zhang et al., 2022). The latter application assumes, implicitly or otherwise, that $BaSO_4$ accurately preserves the primary Ba isotope composition set during mineral formation. However, this assumption has yet to be fully investigated during early diagenesis, that is, during the chemical changes which occur after deposition and burial of the mineral on the seafloor.

Barite diagenesis under anoxic, suboxic, and sulfidic conditions is well studied (Gingele et al., 1999; McManus et al., 1998; Rutsch et al., 1995), and morphological and geochemical criteria exist to screen sedimentary $BaSO_4$ for diagenetic alteration that occurs under these conditions (e.g., Griffith and Paytan, 2012). Under oxic, sulfate-replete conditions, chemical alteration of many sulfate minerals, including $BaSO_4$, has also been observed without visible

* Corresponding author.
E-mail address: jtmiddleton@ucsb.edu (J.T. Middleton).

https://doi.org/10.1016/j.epsl.2023.118150
0012-821X/

changes to crystal morphology (Gorski and Fantle, 2017; Klinkenberg et al., 2014). In these cases, alteration occurs through surface-mediated processes that allow ions to exchange between the mineral and a surrounding fluid without affecting the morphology of the mineral itself (Bosbach et al., 2010; Brandt et al., 2015; Curti et al., 2010; Klinkenberg et al., 2014; Torapava et al., 2014; Vinograd et al., 2013). A recent study showed that the isotope composition of Ba in synthetic $BaSO_4$ is susceptible to alteration through surface-mediated ion exchange under oxic, sulfate-replete ambient conditions (Middleton et al., 2023); however, it is unknown if similar alteration of Ba isotopes occurs for pelagic $BaSO_4$ buried in the oxic, sulfate-replete sediments found in the marine environment.

Here, we investigate the potential of ion-exchange-mediated diagenesis to alter the Ba isotope composition of pelagic $BaSO_4$. To achieve this, we studied the Ba isotope composition of sedimented pelagic $BaSO_4$, co-located porewaters, and the overlying water column in samples collected from the Equatorial Pacific. These sediments offer an ideal opportunity to evaluate the role of ion-exchange-mediated diagenesis, as sedimentary pelagic $BaSO_4$ and porewaters remain in contact over millennia (Murray et al., 1995). We first report results which identify the presence and rate of ion exchange (R_{Ix}) between modern pelagic $BaSO_4$ and seawater using bench-top isotope tracer experiments. These rates were then compared to modeled rates of ion exchange between porewaters and $BaSO_4$ in sediment cores from the Equatorial Pacific. We then constructed a two-box model of porewater-$BaSO_4$ interactions in the sediments, which implies significant fluxes of Ba ions between the mineral and fluid. These fluxes occur with porewaters near chemical equilibrium with respect to $BaSO_4$ and affects the Ba isotope composition of $BaSO_4$ and dissolved Ba in porewaters. The rate of ion exchange, associated rate constants of $BaSO_4$ precipitation, and magnitude of Ba isotope fractionation derived through the model agree well with laboratory results and prior literature. These findings suggest that ion-exchange-mediated diagenesis is an important control on Ba isotope compositions in sedimentary porewaters and, in some environments, co-located $BaSO_4$.

2. Methods

2.1. Field setting and sampling

Field samples were collected in the Equatorial Pacific in 1992 (sediments and porewaters) and 2016 (seawater; Fig. 1). Full sampling protocols for sediment and porewater collected during the Joint Global Ocean Flux Study (JGOFS) TTN013 may be found in Paytan and Kastner (1996). Briefly, sediments were collected using a multi-corer and had well-preserved sediment–water interfaces. Sub cores were transferred to a 2 °C cold room immediately upon arrival onboard and sectioned in a nitrogen atmosphere glovebox. Porewaters were extracted by centrifugation and filtered to 0.45 µm through a pre-washed Nucleopore filter, then acidified to pH 2 with nitric acid. Cores were oxic and sulfate replete over the depth sampled (Paytan and Kastner, 1996). Barite samples were previously separated by Paytan and Kastner (1996). Seawater samples from the ProteOMZ expedition (FK160115; Saunders et al., 2022) were collected using Niskin-X bottles mounted on a trace metal rosette and filtered in a fabricated cleanroom on the ship. Samples were filtered to 0.2 µm through acid-washed polyethersulfone (PES) filters and collected into acid-washed high-density polyethylene (HDPE) bottles, then acidified to pH 2 using hydrochloric acid. Samples were stored for three years prior to analysis. Exact sample coordinates and identifiers are found in Table 1.

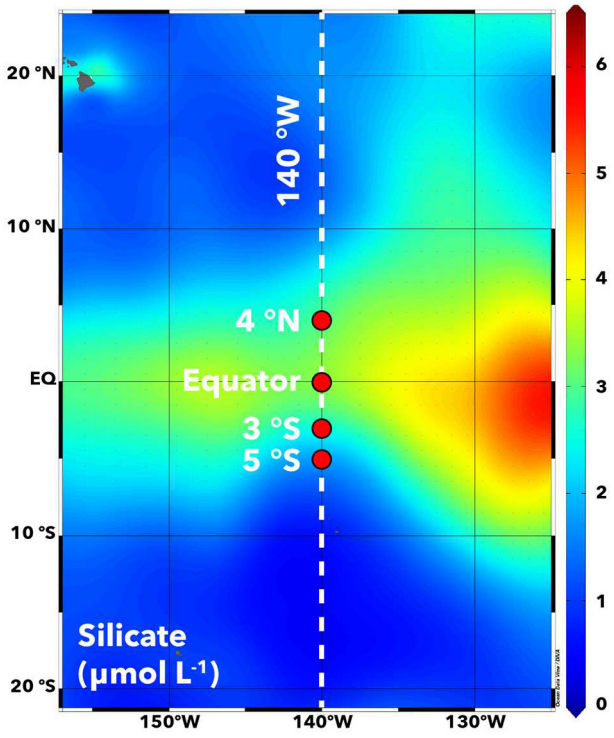

Fig. 1. Sampling sites for the Joint Global Ocean Flux Study (JGOFS) and ProteOMZ projects. Exact sampling coordinates for water column, sediment, and porewater samples are given in Table 1. Surface silicate concentration from World Ocean Atlas (Garcia et al., 2018) is shown as a proxy for dissolved surface [Ba].

2.2. Isotope-tracer experiments

A matrix experiment was carried out to assess the rate of ion exchange between seawater and $BaSO_4$. Two types of seawater were tested—filtered seawater (FSW) from Vineyard Sound, Massachusetts, and artificial seawater (ASW)—as were two types of $BaSO_4$: natural, isolated from Equatorial Pacific sediments, and synthetic (Alfa Aesar $BaSO_4$ powder; Lot #24177). Filtered seawater was used to identify whether Ba ion exchange occurred in natural seawater and whether there were any differences compared to artificial seawater (ASW). Filtered seawater was collected at the Environmental Systems Laboratory at Woods Hole Oceanographic Institution (WHOI) using the flow-through seawater system and collected into 1 L acid-washed HDPE bottles, then filtered through a 0.4 µm acid-washed PES membrane in a clean room. Experimental setup, seawater-, and $BaSO_4$-characteristics are given in Table 2.

The rate of Ba ion exchange between $BaSO_4$ and fluid was quantified following the protocol of Middleton et al. (2023). Briefly, a known quantity of $BaSO_4$ powders were added to a fluid and kept under constant agitation for a period of up to six months. In each experiment, the dissolved pool was amended with a solution enriched in ^{136}Ba, such that $(^{138}Ba{:}^{136}Ba)_{fluid,initial} = 0.35 \pm 0.03$ ($\pm$2SE, $n = 4$). The $BaSO_4$, in contrast, possessed natural Ba isotope abundances (i.e., $^{138}Ba{:}^{136}Ba \approx 9.1$; de Laeter et al., 2003). Thus, if ion exchange were to occur between $BaSO_4$ and dissolved Ba, $(^{138}Ba{:}^{136}Ba)_{fluid}$ would evolve from the initial value toward natural abundances. Barium-136 additions were adjusted to achieve Ω_{barite} of 1.3, calculated using the aqueous geochemical modeling program PHREEQC (Parkhurst and Appelo, 2013). The slight initial oversaturation was intended to limit dissolution of $BaSO_4$, such that changes in $(^{138}Ba{:}^{136}Ba)_{fluid}$ should derive solely from ion exchange. Initial conditions for experiments are shown in Table 2. Aliquots of 2 mL were sampled over 174 d and filtered through a 0.22 µm PES membrane filter prior to analysis of $(^{138}Ba{:}^{136}Ba)_{fluid}$.

Table 1
Sites of porewater, sedimentary $BaSO_4$, and water column data. In some cases, geographically near sites are considered together. This is indicated by the sample group.

Sample group name	Water column				Pore fluid				$BaSO_4$		
	Cruise	Stn	Lat	Long	Cruise	Core	Lat	Long	Core	Lat	Long
4°N	FK 160115	11	4.00	−140.00	JGOFS	MC113	4.04	−139.85	MC113	4.04	−139.85
Eq		12	0.00	−139.80	EqPac	MC48	0.12	−139.74	MC48	0.12	−139.74
5°S		13	−4.23	−142.23	TT013	MC34	−4.97	−139.74	MC27	−2.89	−139.83

Table 2
Initial conditions for isotope-tracer experiments.

ID	Fluid[a]	Barite[b]	Fluid mass (g)	Barite mass (mg)	Initial [Ba] (nmol L^{-1})	±2SE	L_{barite}[c]	Initial $(^{138}Ba/^{136}Ba)_{fluid}$
ASW1	Artificial SW	Synthetic	1018.5	13	282	14	0.9950	0.32
ASW2	Artificial SW	Pelagic	1017.2	15	283	14	0.9956	0.33
FSW1	Filtered SW	Synthetic	1017.4	17	272	14	0.9963	0.38
FSW2	Filtered SW	Pelagic	1016.0	13	273	14	0.9951	0.37

[a] Artificial seawater was prepared following Smith et al. (1975) and brought to pH ≈ 8.1 by the addition of concentrated potassium hydroxide (KOH) solution. Filtered seawater was collected 400 ft offshore from 4.5 m and filtered to 0.4 μm using a Supor polyethersulfone filter.
[b] Synthetic $BaSO_4$ (Puratronic, Alfa Aesar Lot #24177) and marine pelagic $BaSO_4$ from 4°N site (JGOFS TTN013 Stn117 MC7 at 15 cm downcore).
[c] Fraction of Ba_{total} in $BaSO_4$, where $Ba_{total} = Ba_{dissovled} + Ba_{barite}$.

A control experiment was used to assess Ba adsorption onto bottle walls. This experiment was conducted under the same conditions as the isotope-tracer experiments, with two differences: dissolved Ba came from a $BaCl_2 \cdot H_2O$ solution (possessing natural Ba isotope abundances) and no $BaSO_4$ was added. The control experiment was sampled at its initiation and at 180 d.

2.3. Sample preparation and analysis

2.3.1. Sample preparation

Barite samples were dissolved through an alkaline dissolution in perfluoroalkane vials by addition of 1 M Na_2CO_3 solution to form (Ba,Ca)CO_3 as in Breit et al. (1985). The Na_2CO_3 solution was added to achieve $BaSO_4$:Na_2CO_3 of 1:10 by mass, then 18.2 MΩ water was added such that there was 10 mg of $BaSO_4$ per 2 mL of solution. Samples were then sonicated for 60 minutes at room temperature and then heated to 80 °C for ≥16 h. After cooling, the fluid was decanted and two further rounds of Na_2CO_3 addition, sonication, heating, and decantation were performed. Samples were rinsed with 18.2 MΩ water and the remaining solid, $BaCO_3$, dissolved with 2 M HCl. An aliquot of this solution was equilibrated with a ^{135}Ba–^{136}Ba double spike of known concentration to achieve a spike- to sample-derived [Ba] ratio of between 1–2 and reconstituted in 250 μL of 2 M HCl ready for ion-exchange chromatography.

Porewater and seawater samples were prepared for Ba isotope analysis following the procedure outlined in Bates et al. (2017). Briefly, dissolved samples were equilibrated with the double spike and then co-precipitated into (Ba,Ca)CO_3 by drop-wise addition of 1 M Na_2CO_3. The precipitate was then dissolved in 250 μL of 2 M HCl for chromatography.

Barium was purified from matrix elements by passing all samples twice through 500 μL of AG 50W-X8 (200–400 mesh) cation-exchange resin (Bio-Rad), following the protocol described by Horner et al. (2015).

2.3.2. Sample analysis

Purified Ba was analyzed for Ba isotopes using a ThermoFinnigan Neptune multi-collector inductively coupled plasma mass spectrometer in the WHOI Plasma Facility. Isotope compositions were calculated using the three-dimensional geometric interpretation of the double-spike problem (Siebert et al., 2001) with additional processing for isobaric corrections (^{136}Xe and ^{136}Ce on ^{136}Ba, ^{138}Ce and ^{138}La on ^{138}Ba; Horner et al., 2015). Barium isotope compositions were calculated relative to NIST by standard-sample bracketing. Four procedural blanks were found to range from 305 to 489 pg, below the long-term average NIRVANA Labs procedural blank (692 pg). A further four analytical blanks were found to range from 14 to 301 pg. The contribution of the highest blank to the sample with the lowest [Ba] was < 3%. Given the low blank contribution and poor constraints on the true Ba isotope blank value, no blank correction was applied. Barium isotope compositions are reported as deviations in the $^{138}Ba/^{134}Ba$ ratio in a sample relative to the NIST SRM 3104a standard, hereafter 'NIST':

$$\delta^{138}Ba\ (‰) = [(^{138}Ba/^{134}Ba)_{sample}/(^{138}Ba/^{134}Ba)_{NIST} - 1] \times 1000. \quad (1)$$

Uncertainties are reported as either a long-term measurement of uncertainty (±2 SD about the mean; ± 0.03‰, Horner et al., 2015) or pooled 2 SE from n sample analyses, whichever was greater.

Accuracy of isotope measurements was monitored by processing two internal reference materials alongside samples: the Alfa Aesar $BaSO_4$ powder and GEOTRACES SAFe D1 (northeast Pacific seawater; 1,000 m). The $BaSO_4$ and SAFe D1 possessed $\delta^{138}Ba$ = −0.02 ± 0.03‰ and +0.33 ± 0.04‰, in agreement with previous measurements of −0.04 ± 0.07‰ (n = 7, ±2SE; T.J. Horner pers. comm.) and +0.31 ± 0.03‰ (Cao et al., 2020; Geyman et al., 2019; Hsieh and Henderson, 2017), respectively.

A 100 μL aliquot was taken from the isotope tracer subsamples and diluted to 1900 μL with 2% HNO_3 and spiked with 100 μL indium (In)—an internal standard—to achieve a final [In] of 1 ng mL^{-1}. All samples were diluted and measured at a salinity of 1.75 to minimize non-spectral matrix effects. Filtered samples were analyzed for ^{138}Ba:^{136}Ba on a reverse quadrupole ICP-MS (iCAP-RQ, Thermo Fisher Scientific) and measurement uncertainty was calculated to be ± 0.05 in (^{138}Ba:^{136}Ba) space.

3. Results

3.1. Environmental data

3.1.1. Barium in the water column of the equatorial Pacific

Seawater in the Equatorial Pacific show the characteristic vertical profile of $[Ba]_{SW}$, with low surface values (~30 nmol L^{-1}) and higher values at depth (~140 nmol L^{-1}; Fig. 2). In all locations, $[Ba]_{SW}$ is constant in surface waters above ~200 m, where $[Ba]_{SW}$ = 34 ± 1 nmol L^{-1} and $\delta^{138}Ba$ = +0.60 ± 0.01‰ (n = 17, ±2SE)

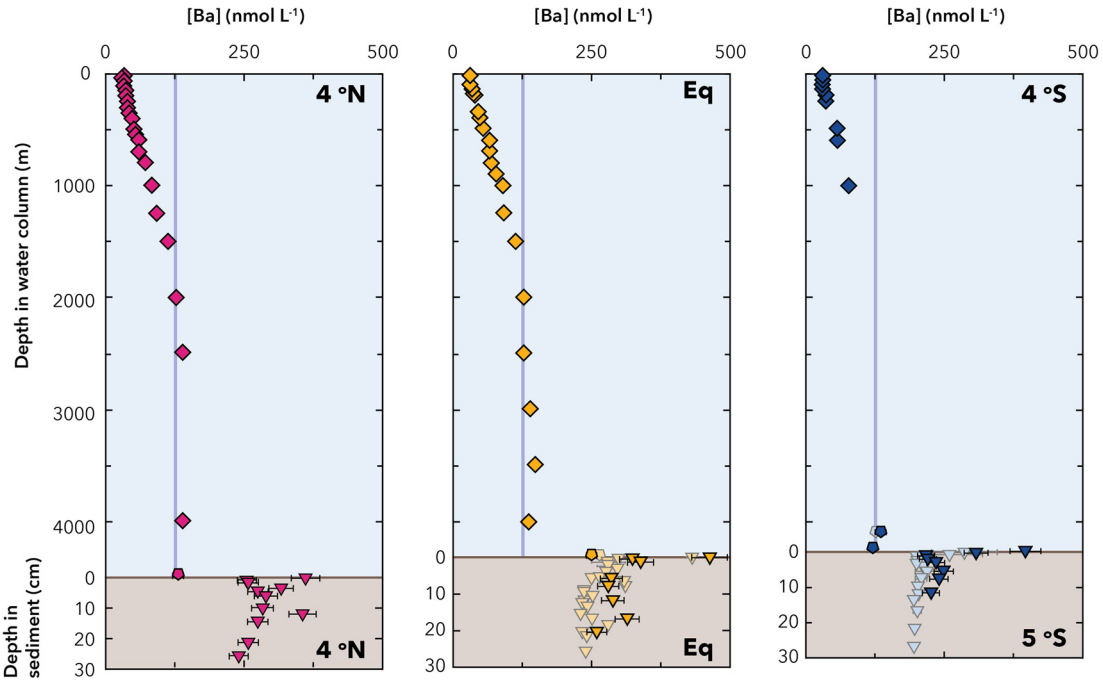

Fig. 2. Ba concentration in the water column (diamonds), bottom water (inverted pentagons), and porewaters (inverted triangles). The mean deep water [Ba] is shown as dark blue shading in the water column. Sampling location of the water column and sediment are notated in the top right and bottom right corners, respectively. Porewater [Ba] originally measured by Paytan and Kastner (1996) are shown in lighter shades in the sediment. The slightly greater [Ba] measured here reflects evaporation during 25 y of storage, with four samples significantly evaporated.

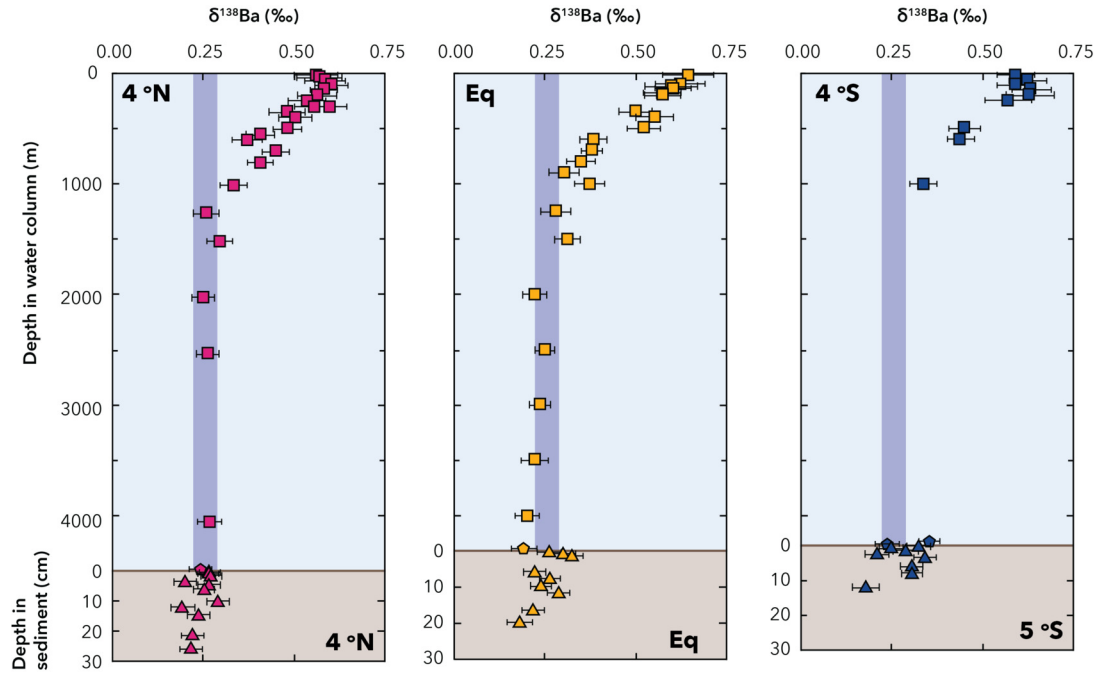

Fig. 3. Ba isotopes in the water column (squares), bottom water (pentagons), and porewaters (triangles). The mean deep water δ^{138}Ba is shown as dark blue shading in the water column. Sampling location of the water column and sediment are notated in the top left and bottom right corners, respectively. Sample evaporation during 25 y of storage does not affect $\delta^{138}Ba_{PW}$.

before decreasing toward deep-water values of $[Ba]_{SW}$ = 125 ± 3 nmol L^{-1} and δ^{138}Ba = +0.26± 0.03‰ (n = 12, ±2SE). Barium concentration profiles in this region co-vary with dissolved silicate, whereby both elements exhibit maxima near 2,500 m (Fig. S1). Values of δ^{138}Ba generally mirror $[Ba]_{SW}$, becoming isotopically heavier as $[Ba]_{SW}$ decreases, in agreement with published profiles (Figs. 2 & 3; Horner et al., 2015); thus, samples from this region also fall along the δ^{138}Ba–1/[Ba] array (Fig. 4).

3.1.2. Barium in the sediments and porewaters of the equatorial Pacific

In the Equatorial Pacific sediments, the δ^{138}Ba of $BaSO_4$ ($\delta^{138}Ba_{barite}$) are consistent between sites with a mean of +0.09 ± 0.03‰ (n = 32, ±2SE; Fig. 5), similar to those of suspended par-

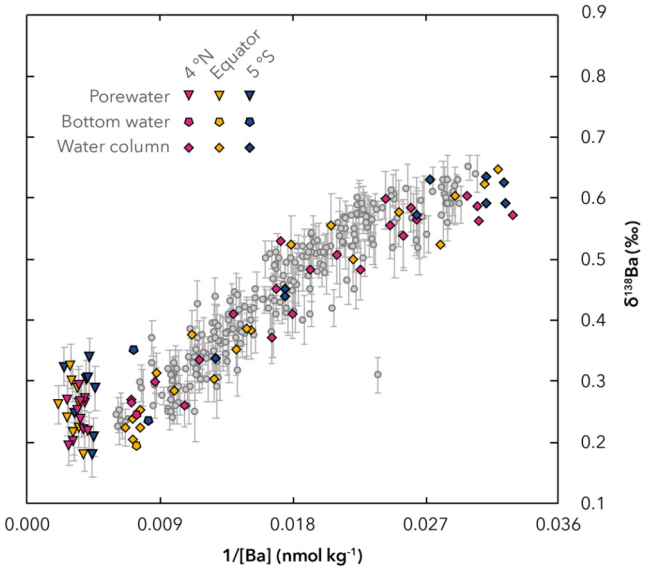

Fig. 4. Global array of 1/[Ba] and δ^{138}Ba in the water column (diamonds) and bottom water (inverted pentagon). Porewaters (inverted triangles) are also plotted. Water column measurements previously made by Horner et al. (2015), Bates et al. (2017), Hsieh and Henderson (2017), Bridgestock et al. (2018), Hemsing et al. (2018), Geyman et al. (2019), and Cao et al. (2020) are in grey. Newly produced water column and bottom water data fall along the global array, whereas porewater data do not.

ticulate Ba (Horner et al., 2017; Cao et al., 2020) and the predicted Ba isotope composition of sedimented pelagic $BaSO_4$ (Bridgestock et al., 2018). Barites are offset from surface waters (0 – 200 m) by $\Delta^{138}Ba_{barite\text{-}dBa} = -0.51 \pm 0.03‰$ ($n = 32$, ±2SE), where $\Delta^{138}Ba_{barite\text{-}dBa} = \delta^{138}Ba_{barite} - \delta^{138}Ba_{dBa}$. This value is in line with the magnitude of fractionation previously observed between pelagic $BaSO_4$ and dissolved Ba in marine environments (Bridgestock et al., 2018; Horner and Crockford, 2021).

Porewater [Ba] ($[Ba]_{PW}$) are similar between sites and agree with previously measured $[Ba]_{PW}$ for the same samples, though four samples exhibited significant evaporation during storage (Fig. 2; Paytan and Kastner, 1996). Excluding these samples, the sites had a mean $[Ba]_{PW}$ of 288 ± 23 (±2SE, $n = 11$), 325 ± 39 (±2SE, $n = 9$), and 261 ± 41 (±2SE, $n = 8$) nmols L^{-1} at 5°S, the Equator, and 4°N, respectively. Porewater profiles exhibit a maximum of ~300–400 nM at the sediment surface before decreasing to a relatively constant value by 1.5 cm core depth (266 ± 21 nmol L^{-1}, $n = 21$, ±2SE).

Porewater δ^{138}Ba ($\delta^{138}Ba_{PW}$) are also similar between sites. Porewaters exhibit mean $\delta^{138}Ba_{PW}$ of +0.28 ± 0.04‰ (±2SE, $n = 11$), +0.26 ± 0.03‰ (±2SE, $n = 9$), and +0.25 ± 0.02‰ (±2SE, $n = 8$) at 5°S, the Equator, and 4°N, respectively (Fig. 3). Seawater Ba isotopes measured within 5 m of the sediment surface were found to be +0.24 ± 0.03‰ (±2SE, $n = 2$), +0.19 ± 0.03‰ (±2SE, $n = 1$), and +0.25 ± 0.03‰ (±2SE, $n = 1$) at 5°S, the Equator, and 4°N, respectively (Fig. 3). These values were similar to core-top $\delta^{138}Ba_{PW}$ at 4°N and 5°S and slightly lower than $\delta^{138}Ba_{PW}$ at the Equator. Notably, $\delta^{138}Ba_{PW}$ is heavier than co-located $\delta^{138}Ba_{barite}$ at all locations by between 0.09 and 0.25‰.

3.2. Isotope-tracer experiments

The rate of Ba ion exchange between $BaSO_4$ and dissolved Ba was quantified through a series of experiments whereby almost all dissolved Ba in ASW was represented by dissolved ^{136}Ba, whereas $BaSO_4$ possessed natural isotope abundances. Initial $(^{138}Ba{:}^{136}Ba)_{fluid}$ was 0.32 ± 0.002 in experiments using ASW ($n = 3$, ±2SE) and 0.36 ± 0.004 in experiments using FSW ($n = 3$, ±2SE). The $(^{138}Ba{:}^{136}Ba)_{solid}$ of the synthetic $BaSO_4$ was 9.13 ± 0.3 ($n = 3$, ± 2SE). Similarly, pelagic $BaSO_4$ had $(^{138}Ba{:}^{136}Ba)_{solid}$ = 9.13 ± 0.01 ($n = 25$, ± 2SE). Adsorption of Ba to vessel walls was assessed using a control trial containing no $BaSO_4$; [Ba] was invariant over 180 days, indicating no significant adsorption (Middleton et al., 2023; Fig. S2). The highly varying proportions of ^{136}Ba and ^{138}Ba in solution preclude the calculation of [Ba] using a conventional external calibration. Instead, we use the total $(^{138}Ba{+}^{136}Ba)_{fluid}$ ion beam intensities, as ion counts per second (CPS), to qualitatively monitor the Ba content of fluids at each timepoint, assess potential changes in $(^{138}Ba{:}^{136}Ba)_{fluid}$ due to any initial dissolution of $BaSO_4$, and monitor the approach to chemical equilibrium. Chemical equilibrium was assumed to occur when [Ba] is no longer changing, which we defined as being the case when at least three consecutive time points had $(^{138}Ba{+}^{136}Ba)_{fluid}$ CPS within analytical uncertainty of one other. In the ASW2, FSW1, and FSW3 trials, the system remained at chemical equilibrium for the duration of the experiment (174 d; Fig. S3). The ASW1 trial reached chemical equilibrium after 2.7 hours following an initial increase in [Ba].

After attaining chemical equilibrium, $(^{138}Ba{:}^{136}Ba)_{fluid}$ of all trials continued to evolve toward $(^{138}Ba{:}^{136}Ba)_{solid}$ (~9.13; Fig. 6). In ASW1 and ASW2, $(^{138}Ba{:}^{136}Ba)_{fluid}$ progressed significantly toward $(^{138}Ba{:}^{136}Ba)_{solid}$ over 174 d, reaching values of 6.34 and 8.44, respectively. The FSW1 and FSW2 trials showed significantly smaller changes in $(^{138}Ba{:}^{136}Ba)_{fluid}$, reaching values of 1.89 and 1.34, respectively. In each experiment, the solid fraction ($BaSO_4$) contained the vast majority of Ba in the system, which we quantify using L_{barite}. Here, L_{barite} refers to the fraction of Ba in the $BaSO_4$–fluid system held by $BaSO_4$. Due to the high L_{barite} of all trials (mean of 0.9955), the fluid phase had little leverage to alter $(^{138}Ba{:}^{136}Ba)_{solid}$ (Table 2). Indeed, at such high L_{barite}, even complete uptake of all dissolved ^{136}Ba into $BaSO_4$ would impart a maximum possible change in $(^{138}Ba{:}^{136}Ba)_{solid}$ of 0.04. As this is the same magnitude as analytical uncertainty, $(^{138}Ba{:}^{136}Ba)_{solid}$ was not monitored over the course of the experiment.

4. Discussion

4.1. Barium isotope equivalence between porewaters and bottom waters: chicken or egg?

The Ba isotope distribution in the water column is thought to be largely set by three processes: $BaSO_4$ formation in surface waters, which preferentially removes isotopically light Ba from seawater with an offset of ≈ −0.5‰, non-fractionating regeneration of $BaSO_4$ at depth, and conservative mixing of water mass δ^{138}Ba and [Ba] along the global overturning circulation (Fig. 3; Horner and Crockford, 2021). Assuming the same processes govern the relationship between $[Ba]_{PW}$ and $\delta^{138}Ba_{PW}$ near chemical equilibrium, we can predict two characteristics of sedimented $BaSO_4$ and associated porewaters in the Equatorial Pacific: 1) that $\delta^{138}Ba_{barite}$ of sedimented pelagic $BaSO_4$ is offset from the overlying surface ocean δ^{138}Ba by $\Delta^{138}Ba_{barite\text{-}dBa} \approx -0.5‰$ (Horner and Crockford, 2021) and 2) $BaSO_4$ dissolution will lead to porewater with $\delta^{138}Ba_{PW} \approx \delta^{138}Ba_{barite}$ across a range of $[Ba]_{PW}$ in the oxic sediments studied here (Murray and Grundmanis, 1980; Paytan and Kastner, 1996). In the first case, the observed overlying water column composition of $\delta^{138}Ba = +0.60 \pm 0.01‰$ ($n = 17$, ±2SE; Fig. 3) is expected to produce pelagic $BaSO_4$ with $\delta^{138}Ba_{barite} \approx +0.10‰$. As expected, $BaSO_4$ measured here have an average value of $\delta^{138}Ba_{barite} = +0.09 \pm 0.03‰$ ($n = 32$, ±2SE; Fig. 5).

However, in the second case, we do not observe the expected result, whereby $\delta^{138}Ba_{PW} = \delta^{138}Ba_{barite}$. Rather, $\delta^{138}Ba_{PW}$ is generally more enriched in heavy Ba isotopes than expected by non-fractionating $BaSO_4$ dissolution, with porewaters offset from co-

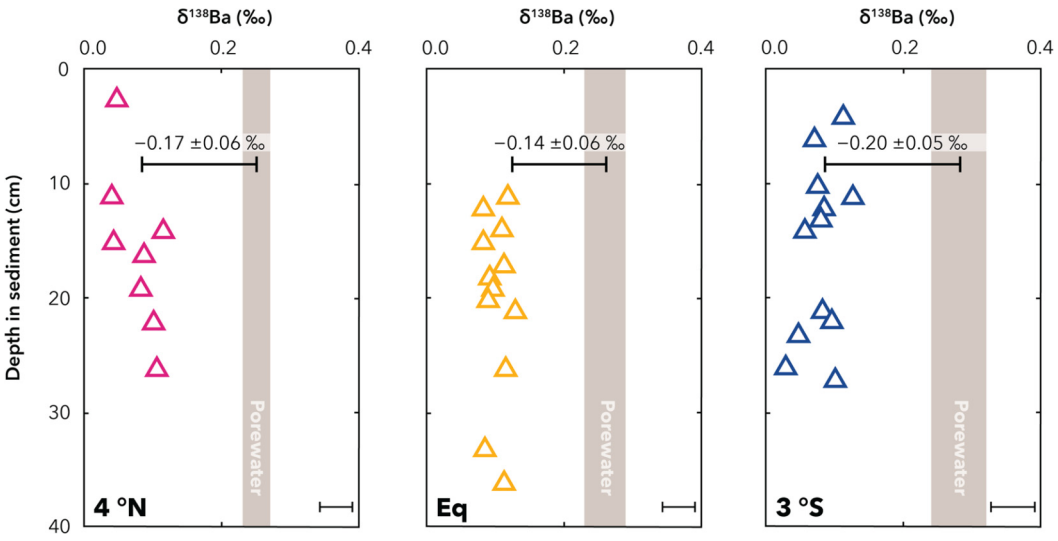

Fig. 5. Ba isotopes of sedimented pelagic $BaSO_4$ from three sites crossing the Equator along the 140°W line. The average uncertainty for measurements from each core is shown in the bottom right of each panel. The Ba isotope composition of $BaSO_4$ is invariant over the depth measured. The mean $\delta^{138}Ba_{PW}$ range is shown in light brown shading and the average $\Delta^{138}Ba_{barite\text{-}dBa}$ of each core is given by the large bracket.

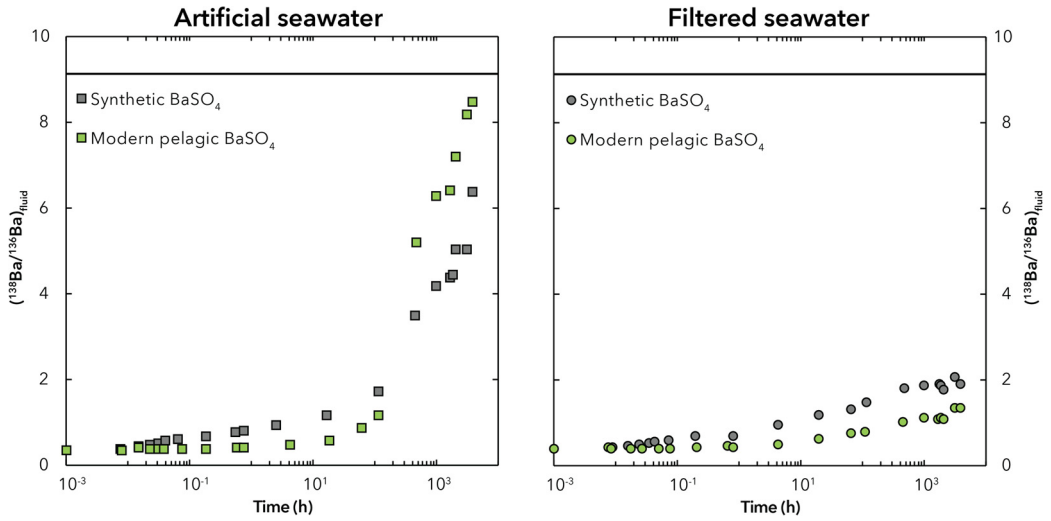

Fig. 6. Temporal evolution of $(^{138}Ba{:}^{136}Ba)_{fluid}$ during Tracer Experiments with aqueous phases at bulk chemical equilibrium conditions. The grey line corresponds to the $(^{138}Ba{:}^{136}Ba)$ of the original BaSO4. Uncertainty of $(^{138}Ba{:}^{136}Ba)_{fluid}$ fall within the points.

located $BaSO_4$ by +0.16 ± 0.04‰ (n = 11, ±2SE) on average (i.e., $\Delta^{138}Ba_{barite\text{-}dBa} = -0.16 \pm 0.04$‰). Intrusion of bottom water (BW) into sediments is unlikely to explain $\delta^{138}Ba_{PW}$ as there is a significant concentration gradient between $[Ba]_{BW}$ (≈125 nM) and $[Ba]_{PW}$ (~300–400 nM). Indeed, Paytan and Kastner (1996) identified that these porewaters were a net source of dissolved Ba to bottom water, consistent with other literature showing a general efflux of dissolved Ba from sediments to overlying bottom water (e.g., McManus et al., 1998). Sustaining the Ba concentration gradient between porewaters and bottom water requires an additional source of Ba to porewaters, such as dissolution of various sedimentary phases (e.g., organic matter, carbonates, $BaSO_4$; Paytan and Kastner, 1996). Porewaters in these particular Equatorial cores are close to chemical equilibrium with respect to $BaSO_4$ after the first few centimeters with no significant change in $\delta^{138}Ba_{barite}$ as $[Ba]_{PW}$ decreases, indicating pelagic $BaSO_4$ as the dominant source of $BaSO_4$, rather than net authigenic precipitation (e.g., Paytan and Kastner, 1996). Thus, the Ba isotope offset between porewaters and co-located $BaSO_4$ requires another process operating in the sediments themselves. One possibility is that there is benthic precipitation of $BaSO_4$ within porewaters. Given a porewater Ba source with $\delta^{138}Ba_{PW}$ ≈+0.25‰, net authigenic precipitation would be expected to drive $\delta^{138}Ba_{barite}$ ≪+0.1‰, unless the fractionation factor was significantly smaller than that previously observed in laboratory and field settings (between −0.3 and −0.5‰). Such a scenario is certainly possible since several studies showed that mineral–fluid isotope fractionation factors are sensitive to the rate of mineral precipitation (DePaolo, 2011), solution chemistry (Tang et al., 2012; Wasylenki et al., 2008), and pressure (Polyakov and Kharlashina, 1994). These effects are, however, unconstrained for Ba in barite–fluid systems.

An alternative explanation is that Equatorial Pacific sedimentary $BaSO_4$ and co-located porewaters are at isotopic equilibrium. Indeed, the observed offset of $\Delta^{138}Ba_{barite\text{-}dBa} = -0.16 \pm 0.04$‰ ($n$ = 11, ±2SE) observed in the Equatorial Pacific sediments is identical, within uncertainty, to that observed for $BaSO_4$ in equilibrium with seawater-like fluids that have undergone significant ion exchange ($\Delta^{138}Ba_{barite\text{-}dBa} = -0.10 \pm 0.05$‰; Middleton et al., 2023). While the similar offsets could be coincidental, it is also possible that ion exchange similarly occurs in Equatorial Pacific sediments. To test this, we performed isotope-tracer experiments

to determine the magnitude and rates of ion exchange between pelagic $BaSO_4$ and seawater, described next.

4.2. Evidence of ion exchange in sedimentary barite from the equatorial Pacific

4.2.1. Isotope-tracer experiments

Isotope-tracer experiments were used to assess whether ion exchange occurred between Equatorial Pacific Pacific $BaSO_4$ and dissolved Ba. To accurately interpret variations in $(^{138}Ba{:}^{136}Ba)_{fluid}$, we first rule out two unrelated processes which may influence $(^{138}Ba{:}^{136}Ba)_{fluid}$: Ba adsorption onto reactor walls and net $BaSO_4$ dissolution. We assume that any net precipitation has a negligible effect on $(^{138}Ba{:}^{136}Ba)_{fluid}$, as the magnitude of change in $(^{138}Ba{:}^{136}Ba)_{fluid}$ is well beyond what is possible by isotope fractionation during $BaSO_4$ precipitation. Dissolved [Ba] remained constant over 180 d in a control experiment, implying that adsorption is negligible (Fig. S2), in agreement with the findings of Heberling et al. (2018). Net $BaSO_4$ dissolution would increase $(^{138}Ba{:}^{136}Ba)_{fluid}$, as $(^{138}Ba{:}^{136}Ba)_{barite} \gg (^{138}Ba{:}^{136}Ba)_{fluid}$ at the start of each experiment. In ASW2, FSW1, and FSW2, [Ba] in the fluid was invariant, indicating no net dissolution of $BaSO_4$ (Fig. S3). In ASW1, Ba in the fluid increased upon $BaSO_4$ addition, indicating net dissolution. We calculated a conservative estimate of the related change in $(^{138}Ba{:}^{136}Ba)_{fluid}$ using a two-endmember isotope mixing equation (see Supplement for full calculation). In ASW1, initial $BaSO_4$ dissolution increased $(^{138}Ba{:}^{136}Ba)_{fluid}$ by 0.27, a small fraction of the final value of 6.34. Thus, having ruled out significant adsorption of Ba to reactor walls and constrained the influence of net $BaSO_4$ dissolution, we interpret further changes in $(^{138}Ba{:}^{136}Ba)_{fluid}$ as representative of ion exchange between dissolved Ba and $BaSO_4$.

For all experiments, $(^{138}Ba{:}^{136}Ba)_{fluid}$ increased toward $(^{138}Ba{:}^{136}Ba)_{barite}$ of ≈9.13 (Fig. 6). The magnitude of the increase was strongly dependent on the nature of the fluid, but not the solid; natural and synthetic $BaSO_4$ behaved similarly to one another in each fluid. That is, ASW1 and ASW2 approached $(^{138}Ba{:}^{136}Ba)_{fluid}$ final values of 6.34 and 8.44 over 174 d, respectively. Comparatively, FSW1 and FSW2 approached final $(^{138}Ba{:}^{136}Ba)_{fluid}$ values of 1.89 and 1.34 over the same time period. For experiments with the same fluid source, differences in final $(^{138}Ba{:}^{136}Ba)_{fluid}$ closely track L_{barite} (Fig. S4). As ion exchange is a surface-mediated process, an increase in apparent exchange rate with available surface area (i.e., L_{barite}) is consistent with previous findings (e.g., Heberling et al., 2018; Middleton et al., 2023; Vital et al., 2020; Zhen-Wu et al., 2016).

We used a numerical model of ion exchange to quantify R_{Ix} (hereafter the "Tracer Model"; see Supplement for a full description). Briefly, R_{Ix} was calculated by fitting fluid data to a time-dependent model of mineral-fluid ion exchange. Tracer Model initialization accounted for reactor-specific parameters, including initial [Ba], solution volume, and the mass of $BaSO_4$. The R_{Ix} was adjusted to minimize the residual sum of squares between experiment data and model output. Ion exchange rates were calculated to encompass the range of $BaSO_4$ crystal diameters observed in the ocean, 0.5 to 5 μm (Yao et al., 2021), and surface area-normalized assuming spherical grains to allow comparison of R_{Ix} between reactors containing differing quantities of $BaSO_4$. The isotope tracer experiments using ASW produce modeled R_{Ix} between 5.3 and 9.7 pmol m^{-2} s^{-1}, in agreement with previous studies (Table 3). In contrast, experiments using FSW exhibited lower R_{Ix} between 0.8 and 1.0 pmol m^{-2} s^{-1}. The reason for slower R_{Ix} in FSW is not immediately apparent, since both the ASW and FSW had similar concentrations of major marine salts and trace metals, L_{barite}, and pH. Given these overall similarities in inorganic chemistry and the similar rate behavior for both natural and synthetic $BaSO_4$, we speculate that the slower rate of exchange in FSW may relate to the presence of dissolved organic matter, which may complex Ba or otherwise influence ion activities at the mineral–fluid interface and inhibit reactivity. Similar organic matter mediated reaction inhibition has been suggested to slow dissolution of calcite (Naviaux et al., 2019). Regardless, our isotope-tracer experiments offer strong evidence of ion exchange in both synthetic and natural $BaSO_4$ and in both ASW and FSW.

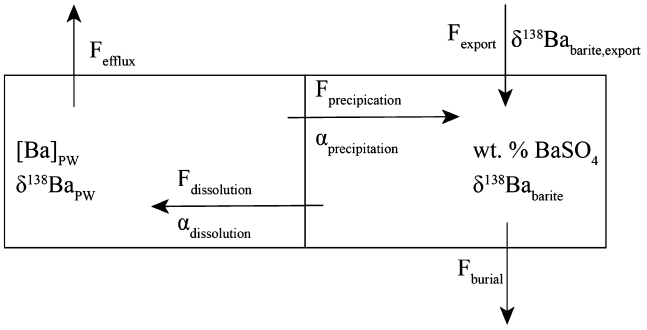

Fig. 7. Box model of Ba cycling in marine sediments. The export of $BaSO_4$ to marine sediments (F_{export}), diffusion of dissolved Ba out of porewaters into bottom water (F_{efflux}), burial of $BaSO_4$ in the sediments (F_{burial}), and dissolution of $BaSO_4$ ($F_{dissolution}$) are parameterized using prior measurements (Table S1). The flux of Ba by precipitation of $BaSO_4$ ($F_{precipitation}$) is used as the fit parameter.

4.2.2. Comparison of ion exchange rates with previous estimates

The isotope-tracer experiments show that Equatorial Pacific $BaSO_4$ incubated in natural seawater at ambient conditions undergo of ion exchange at rates ~1 pmol m^{-2} s^{-1}. We now put these rates into context by comparing them against R_{Ix} calculated by mass balance for the sediments of the Equatorial Pacific sediments and previously measured literature values. First, mass balance calculations using a two-box model in which ion exchange was allowed were used to constrain environmental R_{Ix} (Fig. 7). Calculations assumed: (1) the Ba distribution in the sediments is at steady state; (2) the rates of burial, export, and efflux may be parameterized as described by previous literature for this region (Paytan and Kastner, 1996; Table S1); (3) Ba ion exchange is allowed between $BaSO_4$ and Ba_{PW} and these are the only Ba-phases capable of ion exchange (Fig. S5; see Supplement for full equations). As in the Tracer Model, R_{Ix} was calculated assuming $BaSO_4$ crystal diameters of 0.5 and 5 μm and surface area-normalized assuming spherical grains. As in previous studies, R_{Ix} is taken from the forward rate of Ba exchange into $BaSO_4$ (Bosbach et al., 2010; Curti et al., 2010; Torapava et al., 2014; Brandt et al., 2015; Heberling et al., 2018). For 5 μm grains, environmental R_{Ix} for the 5°S, Equator, and 4°N sediments are 0.51, 0.57, and 0.34 pmol m^{-2} s^{-1}, respectively (Table 3). The modeled environmental R_{Ix} of 0.34 to 0.57 pmol m^{-2} s^{-1} agree well with the Tracer Model results for modern pelagic $BaSO_4$ in FSW of 0.8 pmol m^{-2} s^{-1} (Table 3).

To allow a second point of comparison, the forward rate constant (k_f) was calculated using the rate of ion exchange following the formulation of Kang et al. (2022), where

$$R_{Ix} = k_f \left(\frac{1}{2 \cdot \frac{[Ba]_{PW}}{[SO_4]} \cdot 0.2} + \frac{\frac{[Ba]_{PW}}{[SO_4]} \cdot 0.2}{2} \right)^{-0.25} \times \left(\left(\frac{[Ba]_{PW} \cdot [SO_4]}{k_{sp,barite}} \right)^{0.5} - 1 \right)^2 \times exp\left[\frac{-Ea}{R} \left(\frac{1}{T} - \frac{1}{298.15} \right) \right], \quad (2)$$

with the apparent activation energy Ea = 30 kJ mol^{-1} (Palandri and Kharaka, 2004), the gas constant R, $[SO_4]$ = 29 mM (Blake et

Table 3
Modeled rates of Ba ion exchange (R_{Ix}) into $BaSO_4$ from experimental and field data. High and low estimates for the modeled R_{Ix} represent the rate assuming a $BaSO_4$ crystal diameter of 5 and 0.5 μm, respectively, spanning the range of pelagic $BaSO_4$ crystal sizes (Yao et al., 2021). For previous works, the maximum and minimum R_{Ix} are provided for comparison. However, we note that prior studies investigated Ba ion exchange in far-from-marine conditions. The one exception comes from Curti et al. (2010), whose slowest R_{Ix} occurred in a trial investigating ion exchange at near neutral pH in highly ionic fluids. The rate constant of the forward reaction (k_f) was calculated follow Eq (2) for the 5 μm grain size and represents the upper estimate for this value. Predicated k_f for marine and aquatic environments from Kang et al. (2022) are provided for comparison.

Site	L_{barite}	R_{Ix}, 0.5 μm grains (pmol m^{-2} s^{-1})	± 2SE	R_{Ix}, 5 μm grains (pmol m^{-2} s^{-1})	± 2SE	[Ba]/[SO_4] (nM/mM)	k_f (pmol m^{-2} s^{-1})	$\Delta^{138}Ba_{barite\text{-}dBa}$ (‰)	± 2SE
ASW, synthetic $BaSO_4$	0.9949	0.53		5.3					
ASW, modern pelagic $BaSO_4$	0.9956	1.0		9.7					
FSW, synthetic $BaSO_4$	0.9963	0.10		1.0					
FSW, modern pelagic $BaSO_4$	0.9951	0.08		0.8					
5°S, JGOFS TT013 MC34	0.9993	0.05	0.001	0.51	0.01	1.20E-05	21.2	−0.14	0.20
Equator, JGOFS TT013 MC48	0.9998	0.06	0.001	0.57	0.01	1.20E-05	8.8	−0.12	0.60
4°N, JGOFS TT013 MC113	0.9998	0.03	0.001	0.34	0.01	1.20E-05	7.8	−0.18	0.50
Curti et al. (2010)	0.9900			28	16				
	0.9974			567	255				
Torapava et al. (2014)	0.99998			174					
	0.99996			694					
Brandt et al. (2015)	Not reported			5					
	Not reported			4630					
Heberling et al. (2018)	Not reported			110	60				
	Not reported			1400	200				
Kang et al. (2022)				Seawater		3.87E-06	0.8		
				Groundwater		4.66E-04	46.0		
				River water		3.78E-03	175.0		

al., 2006), and temperature and pressure corrected pk_{sp} = −8.39 (Rushdi et al., 2000). Using this formulation, k_f for the 5°S, Equator, and 4°N sites are 21.2, 8.8, and 7.8 pmol m^{-2} s^{-1} and fall between k_f predicted for seawater and groundwater (Kang et al., 2022; Table 3). The agreement between modeled R_{Ix} in sediment cores and experiments, combined with the agreement between calculated and predicted k_f, suggests that ion exchange of Ba occurs between porewaters and $BaSO_4$ in the Equatorial Pacific.

4.2.3. Evaluation of the significance of ion exchange in equatorial Pacific barites

We now assess the potential impact of ion exchange on $\delta^{138}Ba_{PW}$ and $\delta^{138}Ba_{barite}$ by performing an isotope mass balance calculation that considers the above-calculated rates and ambient $[Ba]_{PW}$. The isotope mass balance calculation assumes that (1) the isotope compositions of the porewaters and $BaSO_4$ are at steady state, (2) the forward reaction, $BaSO_4$ precipitation, fractionates Ba isotopes with $\alpha_{precip.}$ = 0.99968±0.00002 (where $\alpha = (^{138}Ba/^{134}Ba)_{product}/(^{138}Ba/^{134}Ba)_{reactant}$; von Allmen et al., 2010), (3) sinking pelagic $BaSO_4$ has a Ba isotope composition of +0.10‰ (Horner et al., 2017; Cao et al., 2020), and (4) the system is at Ba isotopic equilibrium with respect to ion exchange. With regards to the fourth assumption, it is important to remember that other mineral phases, including clays, likely adsorb some fraction of $[Ba]_{PW}$. This is an important process and may fractionate Ba isotopes in the porewaters at the time of occurrence. However, Ba adsorption onto riverine particulates has been shown to be rapid and Ba desorption has not been found to significantly occur in the absence of large salinity changes (Bridgestock et al., 2021; Gou et al., 2020). Given that these sediments appear to maintain a constant $\Delta^{138}Ba_{barite\text{-}dBa}$ over the millennia represented by the core depth investigated here (Murray et al., 1995) and that the down core porewater salinity can be assumed to be relatively constant over these core depths in the Equatorial Pacific (as in Hammond et al., 1996), we evaluate Ba isotope fractionation with respect to $BaSO_4$-fluid ion exchange alone. Using the modeled environmental R_{Ix}, steady state mass balance of $\delta^{138}Ba_{PW}$ and $\delta^{138}Ba_{barite}$ necessitates micro-scale dissolution of $BaSO_4$ related to ion exchange to fractionate Ba isotopes with an average magnitude of $\alpha_{diss.}$ = 0.99985±0.00006 (n = 3, ± 2SE; Table 3). This value is consistent with the findings of Middleton et al. (2023), where $BaSO_4$ dissolution was predicted to have $\alpha_{diss.}$ = 0.99978±0.00006. The combined effect of micro-scale precipitation and dissolution during ion exchange imparts a modeled offset of $\Delta^{138}Ba_{barite\text{-}dBa}$= −0.17‰. Further study is needed to interrogate the role of reaction rate, porewater chemistry, and pressure effects. Given the agreement of R_{Ix}, k_f, and $\alpha_{diss.}$ with previous findings (Kang et al., 2022; Middleton et al., 2023), we suggest that $BaSO_4$-fluid ion exchange plays a role in setting $\Delta^{138}Ba_{barite\text{-}dBa}$ in these sediments.

While these results suggest that ion exchange has a role in mediating sedimentary Ba isotope behavior, our results do not resolve the mechanism of Ba isotope fractionation predicted during $BaSO_4$ dissolution. In general, the mechanism of dissolution can affect isotope fractionation (e.g., Kiczka et al., 2010; Wetzel et al., 2014; Wiederhold et al., 2006) and it is noteworthy that previous studies found $BaSO_4$ dissolution mediated by Na_2CO_3 is non-fractionating when >10% of the mineral dissolves (van Zuilen et al., 2016; von Allmen et al., 2010). However, carbonate-for-sulfate substitution and witherite ($BaCO_3$) formation is unlikely in these cores given the much lower carbonate ion concentrations compared to the hot alkaline solutions used to dissolve $BaSO_4$ for subsequent isotope analysis. Further study is needed to directly constrain the magnitude of Ba isotope fractionation during $BaSO_4$ dissolution under marine-relevant conditions.

4.3. Implications for barite-based proxies

4.3.1. Barium isotopes in barite

Use of $\delta^{138}Ba_{barite}$ as a proxy for past seawater $\delta^{138}Ba$ assumes that the isotope composition of Ba recorded by $BaSO_4$ remains unchanged over time. While ion exchange appears to affect $\delta^{138}Ba_{PW}$, as discussed in Sections 4.2.3, the high L_{barite} in the sediments of

the Equatorial Pacific ensures only minimal change of $\delta^{138}Ba_{barite}$. Such systems are likely to remain viable for proxy applications for considerable spans of time. Specifically, mass balance calculations indicate that in systems with a degree of isotopic disequilibrium similar to that observed in the present study, sediments with L_{barite} >0.78 are protected from measurable changes in $\delta^{138}Ba_{barite}$, as the total $\delta^{138}Ba$ of the system is strongly controlled by the solid. Assuming no advection of porewaters, all cores in this study have L_{barite} > 0.99 (Table 3). However, should dissolved Ba in porewaters undergo some amount of turnover, the effective L_{barite} in the system may be lower, as new input of $[Ba]_{PW}$ reduces the relative leverage of $BaSO_4$. In such a scenario, $\delta^{138}Ba_{barite}$ may be vulnerable to change after deposition. Marine sediments with high overturning of $[Ba]_{PW}$ include those experiencing diffusive fluxes (McManus et al., 1998), hydrothermal (Snelgrove and Forster, 1996) or cold seep circulation (Hu et al., 2019; Rooze et al., 2020), and submarine groundwater discharge (Hong et al., 2019). In the cores studied here, $[Ba]_{PW}$ must overturn between ~3,000 – 16,000 times to lower L_{barite} from ~0.995 to 0.78. Based on the Ba efflux rate for these sediments (~14 nmols cm^{-2} y^{-1}; Paytan and Kastner, 1996; McManus et al., 1998), overturning of the dissolved Ba pool may occur over a timespan of 40–250 years. Accounting for this overturning can shift the modeled offset at isotopic equilibrium between $\delta^{138}Ba_{barite}$ and $\delta^{138}Ba_{PW}$ from −0.17 to −0.15‰. It should be noted that these time spans represent the most rapid overturning of the dissolved Ba pool possible in the system, especially since large diffusive fluxes are not expected downcore, where $[Ba]_{PW}$ is relatively constant.

Maintaining effective leveraging of L_{barite} >0.78 will generally allow sedimented pelagic $BaSO_4$ to faithfully retain its initial Ba isotope composition that reflects surface-ocean conditions. However, estimating L_{barite} may be challenging in systems where no co-existing porewaters are available, such as for ancient rocks or if no porewaters were collected. We suggest two paths forward. First, one might use radiogenic strontium (Sr) isotopes in sedimented $BaSO_4$ to screen for low L_{barite}. As with Ba, $BaSO_4$ also records ambient seawater $^{87}Sr/^{86}Sr$ at the time of precipitation (e.g., Paytan et al., 1993). Strontium, being a chemically similar element to Ba, is also likely to undergo ion-exchange-mediated diagenesis. Thus, $BaSO_4$ that have undergone considerable ion exchange will exhibit $^{87}Sr/^{86}Sr$ that differs from the ratio expected of $BaSO_4$ of that age. Such $BaSO_4$ are also unlikely to be suitable for reconstructing $\delta^{138}Ba_{SW}$. Second, if Sr isotope screening is not possible, we suggest avoiding over-interpreting down-core variations in $\delta^{138}Ba_{barite}$ that are smaller than 0.17‰, as such changes fall within the range of Ba isotope variation attributable solely to ion-exchange-mediated diagenesis.

4.3.2. Trace elements in barite

The finding of Ba ion exchange between dissolved Ba in porewaters and sedimented pelagic $BaSO_4$ suggests that other isotope systems measured in $BaSO_4$ may also be affected, particularly those that are chemically similar to Ba. Radium (Ra) is one such element, with ^{226}Ra commonly measured in $BaSO_4$ to construct sediment age models. This chronometer assumes that $BaSO_4$ acts as a closed system with respect to Ra (i.e., Ra ion exchange does not occur). Indeed, previous studies observed that downcore profiles of $[^{226}Ra]$ in Equatorial Pacific $BaSO_4$ showed exponentially decreasing concentrations, which was interpreted to reflect closed-system behavior (e.g., Paytan et al., 1996). Such behavior seems likely if Ba *and* Ra ion exchange are occurring concurrently (e.g., Heberling et al., 2018) and thus we suggest an alternative explanation that is consistent with co-occurring Ba and Ra ion exchange. In the original study, Paytan et al. (1996) suggested closed system behavior due to sedimented $BaSO_4$ exhibiting surface water $^{230}Th/^{232}Th$ values, $^{226}Ra/Ba$ ratios in $BaSO_4$ remaining lower than expected if a partition coefficient (D_{Ra}) of 1 is assumed, and the Ra decay product radon (^{222}Rn) appearing anomalously low despite no known escape mechanism. Subsequent work has challenged these underlying assumptions: Ra ion exchange with $BaSO_4$ is known to occur (Bosbach et al., 2010; Curti et al., 2010), Ra partitioning into $BaSO_4$ during ion exchange exhibits D_{Ra} as low as 0.08 (Curti et al., 2010), and ^{222}Rn is known to preferentially escape $BaSO_4$ during ^{226}Ra decay (Hosoda et al., 2016). Thus, an alternative explanation is that the aforementioned processes were occurring within a reactive system whereby total ^{226}Ra was dominated by that in $BaSO_4$. A $BaSO_4$-leveraged system would be expected to produce the same decay trends as the case where $BaSO_4$ acts as a closed system, even if rapid exchange of Ra were occurring between porewaters and $BaSO_4$, as originally suggested by Church and Bernat (1972). Even if ion exchange of Ra were occurring, the ^{226}Ra content of $BaSO_4$ still offers a valuable means for constructing age models so long as the total ^{226}Ra content of the system is dominated by the ^{226}Ra content of $BaSO_4$. Additional study is needed to quantify the impact of ion exchange on ^{226}Ra in sedimented $BaSO_4$. Likewise, ion exchange may affect the partitioning and isotopic composition of other chemically similar elements in $BaSO_4$ such as Ca and Sr. Ideally, such effects should be studied across a range of L_{barite}.

5. Conclusions

We present results suggesting that ion exchange—coupled surface-mediated precipitation–dissolution—occurs between porewaters and pelagic $BaSO_4$ in Equatorial Pacific sediments at chemical equilibrium. These interpretations were derived using data from field samples and laboratory experiments. Field samples show that sedimented pelagic $BaSO_4$ are offset relative to co-located porewaters by −0.16 ± 0.04‰ and that porewaters and bottom seawater exhibit Ba isotope equivalence. These observations are difficult to reconcile with our current understanding of the marine Ba cycle. Using a series of isotope labeled lab experiments, we show that pelagic $BaSO_4$ undergoes extensive Ba isotope exchange with ambient fluids at chemical equilibrium. The rate of exchange was found to depend on the nature of the fluid, proceeding more slowly in natural, rather than artificial seawater, though not on the solid, occurring at similar rates in both natural and synthetic $BaSO_4$. The observed ion exchange rates of 0.03–0.57 pmol m^{-2} s^{-1} are both geologically reasonable and consistent with previous lab-based estimates. Using estimates of Ba isotope fractionation during precipitation and dissolution, we show that ion exchange can impart small but measurable changes in the Ba isotope composition of porewaters and $BaSO_4$. These changes occur because the processes of precipitation and dissolution impart opposing, but unequal Ba isotope effects which result in a modeled offset of $\Delta^{138}Ba_{barite\text{-}dBa} = -0.17$‰ when isotopic equilibrium is reached. The net result is that $BaSO_4$ and porewaters that achieve isotopic equilibrium through ion exchange will exhibit this characteristic offset ‰. We thus propose that the process of ion exchange explains the Ba isotope offset between $BaSO_4$ and co-located porewaters in the Equatorial Pacific. If correct, our results imply that ion exchange can alter the Ba isotope composition of sedimentary $BaSO_4$. The extent to which this effect will manifest in natural samples will depend on the degree of isotopic disequilibrium and on the fraction of the total Ba in the barite–fluid system that is present in $BaSO_4$ (i.e., the leverage). Systems with high leverage should be robust to ion exchange-mediated alteration over geological timescales, whereas systems with low leverage will not. A number of potential screening criteria are suggested, though we acknowledge that in some settings it may be impossible to constrain leverage. In such systems one should avoid over interpreting temporal variations in $\delta^{138}Ba_{barite}$ <0.17‰, as this would fall within the range of variation that could derive solely through

ion exchange. More broadly, our study adds to a growing body of evidence indicating that ion-exchange-mediated processes are widespread in marine geochemistry and that this process likely impacts other metals and minerals beyond Ba and $BaSO_4$.

CRediT authorship contribution statement

J.T. Middleton: Conceptualization, Data curation, Formal analysis, Investigation, Methodology, Resources, Software, Validation, Visualization, Writing – original draft, Writing – review & editing. **A. Paytan:** Funding acquisition, Resources, Writing – review & editing. **M. Auro:** Writing – review & editing. **M.A. Saito:** Funding acquisition, Writing – review & editing. **T.J. Horner:** Conceptualization, Funding acquisition, Methodology, Resources, Supervision, Visualization, Writing – review & editing.

Declaration of competing interest

The authors declare that they have no known competing financial interests or personal relationships that could have appeared to influence the work reported in this paper.

Data availability

All data are included in the Supplement.

Acknowledgements

Thanks to Jurek Blusztajn and Gretchen Swarr for assistance with mass spectrometry, to the crews of TTN013 (JGOFS) and FK160115 (ProteOMZ on the R/V Falkor supported by the Schmidt Ocean Institute) for facilitating sample collection. This research was made possible by grants from the National Science Foundation: a GRFP grant to J.T.M., OCE-1827431 to A.P., and OCE-1827401 and OCE-2023456 to T.J.H. from the National Science Foundation.

Appendix A. Supplementary material

Supplementary material related to this article can be found online at https://doi.org/10.1016/j.epsl.2023.118150.

References

Bates, S.L., Hendry, K.R., Pryer, H.v., Kinsley, C.W., Pyle, K.M., Woodward, E.M.S., Horner, T.J., 2017. Barium isotopes reveal role of ocean circulation on barium cycling in the Atlantic. Geochim. Cosmochim. Acta 204, 286–299. https://doi.org/10.1016/j.gca.2017.01.043.

Bosbach, D., Böttle, M., Metz Karlsruher, V., 2010. Experimental study on Ra2+ uptake by barite ($BaSO_4$). Stockholm, Sweden.

Brandt, F., Curti, E., Klinkenberg, M., Rozov, K., Bosbach, D., 2015. Replacement of barite by a (Ba, Ra)SO_4 solid solution at close-to-equilibrium conditions: a combined experimental and theoretical study. Geochim. Cosmochim. Acta 155, 1–15. https://doi.org/10.1016/j.gca.2015.01.016.

Breit, G.N., Simmons, E.C., Goldhaber, M.B., 1985. Dissolution of barite for the analysis of strontium isotopes and other chemical and isotopic variations using aqueous sodium carbonate. Chem. Geol. 52, 333–336.

Bridgestock, L., Hsieh, Y. Te, Porcelli, D., Henderson, G.M., 2019. Increased export production during recovery from the Paleocene–Eocene thermal maximum constrained by sedimentary Ba isotopes. Earth Planet. Sci. Lett. 510, 53–63. https://doi.org/10.1016/j.epsl.2018.12.036.

Bridgestock, L., Hsieh, Y. Te, Porcelli, D., Homoky, W.B., Bryan, A., Henderson, G.M., 2018. Controls on the barium isotope compositions of marine sediments. Earth Planet. Sci. Lett. 481, 101–110. https://doi.org/10.1016/j.epsl.2017.10.019.

Bridgestock, L., Nathan, J., Paver, R., Hsieh, Y. Te, Porcelli, D., Tanzil, J., Holdship, P., Carrasco, G., Annammala, K.V., Swarzenski, P.W., Henderson, G.M., 2021. Estuarine processes modify the isotope composition of dissolved riverine barium fluxes to the ocean. Chem. Geol. 579. https://doi.org/10.1016/j.chemgeo.2021.120340.

Cao, Z., Rao, X., Yu, Y., Siebert, C., Hathorne, E.C., Liu, B., Wang, G., Lian, E., Wang, Z., Zhang, R., Gao, L., Wei, G., Yang, S., Dai, M., Frank, M., 2021. Stable barium isotope dynamics during estuarine mixing. Geophys. Res. Lett. 48. https://doi.org/10.1029/2021GL095680.

Cao, Z., Siebert, C., Hathorne, E.C., Dai, M., Frank, M., 2020. Corrigendum to "Constraining the oceanic barium cycle with stable barium isotopes". Earth Planet. Sci. Lett. 434, 1–9. Earth Planet. Sci. Lett. 530, 1–5. https://doi.org/10.1016/j.epsl.2015.11.017 (2016).

Church, T.M., Bernat, M., 1972. Thorium and uranium in marine barite. Earth Planet. Sci. Lett. 14, 139–144.

Crockford, P.W., Wing, B.A., Paytan, A., Hodgskiss, M.S.W., Mayfield, K.K., Hayles, J.A., Middleton, J.E., Ahm, A.S.C., Johnston, D.T., Caxito, F., Uhlein, G., Halverson, G.P., Eickmann, B., Torres, M., Horner, T.J., 2019. Barium-isotopic constraints on the origin of post-Marinoan barites. Earth Planet. Sci. Lett. 519, 234–244. https://doi.org/10.1016/j.epsl.2019.05.018.

Curti, E., Fujiwara, K., Iijima, K., Tits, J., Cuesta, C., Kitamura, A., Glaus, M.A., Müller, W., 2010. Radium uptake during barite recrystallization at 23 ± 2 °C as a function of solution composition: an experimental 133Ba and 226Ra tracer study. Geochim. Cosmochim. Acta 74, 3553–3570. https://doi.org/10.1016/j.gca.2010.03.018.

de Laeter, J.R., Böhlke, J.K., de Bievre, P., Hidaka, H., Peiser, H.S., Rosman, K.J.R., Taylor, P.D.P., 2003. Atomoic weights of the elements (IUPAC review). Pure Appl. Chem. 75, 683–800.

DePaolo, D.J., 2011. Surface kinetic model for isotopic and trace element fractionation during precipitation of calcite from aqueous solutions. Geochim. Cosmochim. Acta 75, 1039–1056. https://doi.org/10.1016/j.gca.2010.11.020.

Dymond, J., Lyle, M., York, N., 1992. Barium in deep-sea sediment: a geochemical proxy for paleoproductivity. Paleoceanography 7, 163–181.

Garcia, H., Weathers, K., Paver, C., Smolyar, I., Boyer, T., Locarnini, R., Zweng, M., Mishonov, V., Baranova, O., Seidov, D., Reagan, J., 2018. Dissolved Inorganic Nutrients (phosphate, nitrate and nitrate+nitrite, silicate). World Ocean Atlas.

Geyman, B.M., Ptacek, J.L., LaVigne, M., Horner, T.J., 2019. Barium in deep-sea bamboo corals: phase associations, barium stable isotopes, & prospects for paleoceanography. Earth Planet. Sci. Lett. 525. https://doi.org/10.1016/j.epsl.2019.115751.

Gingele, F.X., Zabel, M., Kasten, S., Bonn, W.J., Nürnberg, C.C., 1999. Biogenic barium as a proxy for paleoproductivity: methods and limitations of application. In: Use of Proxies in Paleoceanography. Springer, Berlin Heidelberg, pp. 345–364.

Gorski, C.A., Fantle, M.S., 2017. Stable mineral recrystallization in low temperature aqueous systems: a critical review. Geochim. Cosmochim. Acta 198, 439–465. https://doi.org/10.1016/j.gca.2016.11.013.

Gou, L.F., Jin, Z., Galy, A., Gong, Y.Z., Nan, X.Y., Jin, C., Wang, X.D., Bouchez, J., Cai, H.M., Chen, J. bin, Yu , H.M., Huang, F., 2020. Seasonal riverine barium isotopic variation in the middle Yellow River: sources and fractionation. Earth Planet. Sci. Lett. 531. https://doi.org/10.1016/j.epsl.2019.115990.

Griffith, E.M., Paytan, A., 2012. Barite in the ocean - occurrence, geochemistry and palaeoceanographic applications. Sedimentology 59, 1817–1835. https://doi.org/10.1111/j.1365-3091.2012.01327.x.

Guo, H., Li, W.-Y., Nan, X., Huang, F., 2020. Experimental evidence for light Ba isotopes favouring aqueous fluids over silicate melts. Geochem. Perspect. Lett., 6–11. https://doi.org/10.7185/geochemlet.2036.

Hammond, D.E., Mcmanus, J., Berelson, W.M., Kilgore, T.E., Pope-T, R.H., 1996. Early diagenesis of organic material in equatorial Pacific sediments: stoichiometry and kinetics. Deep-Sea Res., Part 2 43, 1365–1412.

Heberling, F., Metz, V., Böttle, M., Curti, E., Geckeis, H., 2018. Barite recrystallization in the presence of 226Ra and 133Ba. Geochim. Cosmochim. Acta 232, 124–139. https://doi.org/10.1016/j.gca.2018.04.007.

Hemsing, F., Hsieh, Y. Te, Bridgestock, L., Spooner, P.T., Robinson, L.F., Frank, N., Henderson, G.M., 2018. Barium isotopes in cold-water corals. Earth Planet. Sci. Lett. 491, 183–192. https://doi.org/10.1016/j.epsl.2018.03.040.

Hodgskiss, M.S.W., Crockford, P.W., Peng, Y., Wing, B.A., Horner, T.J., 2019. A productivity collapse to end Earth's great oxidation. Proc. Natl. Acad. Sci. USA 116, 17207–17212. https://doi.org/10.1073/pnas.1900325116.

Hong, W.L., Lepland, A., Himmler, T., Kim, J.H., Chand, S., Sahy, D., Solomon, E.A., Rae, J.W.B., Martma, T., Nam, S. il, Knies, J., 2019. Discharge of meteoric water in the eastern Norwegian sea since the last glacial period. Geophys. Res. Lett. 46, 8194–8204. https://doi.org/10.1029/2019GL084237.

Horner, T.J., Crockford, P.W., 2021. Barium isotopes in barite: drivers, dependencies, and distributions through space and time geochemical tracers in Earth system science. In: Geochemical Tracers in Earth System Science, pp. 1–29.

Horner, T.J., Kinsley, C.W., Nielsen, S.G., 2015. Barium-isotopic fractionation in seawater mediated by barite cycling and oceanic circulation. Earth Planet. Sci. Lett. 430, 511–522. https://doi.org/10.1016/j.epsl.2015.07.027.

Horner, T.J., Pryer, H.v., Nielsen, S.G., Crockford, P.W., Gauglitz, J.M., Wing, B.A., Ricketts, R.D., 2017. Pelagic barite precipitation at micromolar ambient sulfate. Nat. Commun. 8. https://doi.org/10.1038/s41467-017-01229-5.

Hosoda, M., Kelleher, K., Murray, M., McGinnity, P., Hanley, O., Wong, J., Currivan, L., 2016. Measurement of 222Rn flux, 222Rn emanation, and 226,228Ra concentration from injection well pipe scale. Radiat. Envrion. Med. 5, 22–28.

Hsieh, Y. Te, Bridgestock, L., Scheuermann, P.P., Seyfried, W.E., Henderson, G.M., 2021. Barium isotopes in mid-ocean ridge hydrothermal vent fluids: a source of isotopically heavy Ba to the ocean. Geochim. Cosmochim. Acta 292, 348–363. https://doi.org/10.1016/j.gca.2020.09.037.

Hsieh, Y. Te, Henderson, G.M., 2017. Barium stable isotopes in the global ocean: tracer of Ba inputs and utilization. Earth Planet. Sci. Lett. 473, 269–278. https://doi.org/10.1016/j.epsl.2017.06.024.

Hu, Y., Luo, M., Liang, Q., Chen, L., Feng, D., Yang, S., Liang, J., Chen, D., 2019. Pore fluid compositions and inferred fluid flow patterns at the Haima cold seeps of the South China Sea. Mar. Pet. Geol. 103, 29–40. https://doi.org/10.1016/j.marpetgeo.2019.01.007.

Kang, J., Bracco, J.N., Rimstidt, J.D., Zhu, G.H., Huang, F., Zhu, C., 2022. Ba attachment and detachment fluxes to and from barite surfaces in 137Ba-enriched solutions with variable [Ba2+]/[SO42−] ratios near solubility equilibrium. Geochim. Cosmochim. Acta 317, 180–200. https://doi.org/10.1016/j.gca.2021.11.008.

Kiczka, M., Wiederhold, J.G., Frommer, J., Kraemer, S.M., Bourdon, B., Kretzschmar, R., 2010. Iron isotope fractionation during proton- and ligand-promoted dissolution of primary phyllosilicates. Geochim. Cosmochim. Acta 74, 3112–3128. https://doi.org/10.1016/j.gca.2010.02.018.

Klinkenberg, M., Brandt, F., Breuer, U., Bosbach, D., 2014. Uptake of Ra during the recrystallization of barite: a microscopic and time of flight-secondary ion mass spectrometry study. Environ. Sci. Technol. 48, 6620–6627. https://doi.org/10.1021/es405502e.

McManus, J., Berelson, W.M., Klinkhammer, G.P., Johnson, K.S., Coale, K.H., Anderson, R.F., Kumar, N., Burdige, D.J., Hammond, D.E., Brumsack, H.J., Mccorkle, D.C., Rushdi, A., 1998. Geochemistry of barium in marine sediments: implications for its use as a paleoproxy. Geochim. Cosmochim. Acta 62, 3453–3473.

Middleton, J.T., Hong, W.-L., Paytan, A., Auro, M.E., Griffith, E.M., Horner, T.J., 2023. Barium isotope fractionation in barite–fluid systems at chemical equilibrium. Chem. Geol. 627, 121453.

Murray, J.W., Grundmanis, V., 1980. Oxygen consumption in pelagic marine sediments. Science 1979 (209), 1527–1530.

Murray, R.W., Leinen, M., Murray, D.W., Mix, A.C., Knowlton, C.W., 1995. Terrigenous Fe input and biogenic sedimentation in the glacial and interglacial equatorial Pacific Ocean. Glob. Biogeochem. Cycles 9, 667–684.

Naviaux, J.D., Subhas, A.v., Dong, S., Rollins, N.E., Liu, X., Byrne, R.H., Berelson, W.M., Adkins, J.F., 2019. Calcite dissolution rates in seawater: lab vs. in-situ measurements and inhibition by organic matter. Mar. Chem. 215, 1–14. https://doi.org/10.1016/j.marchem.2019.103684.

Palandri, J.L., Kharaka, Y.K., 2004. A Compilation of Rate Parameters of Water-Mineral Interaction Kinetics for Application to Geochemical Modeling. U.S. Geological Survey, Menlo Park, CA.

Parkhurst, D., Appelo, C., 2013. Description of input and examples for PHREEQC version 3: a computer program for speciation, batch-reaction, one-dimensional transport, and inverse geochemical calculations. Denver, CO.

Paytan, A., Griffith, E.M., 2007. Marine barite: recorder of variations in ocean export productivity. Deep-Sea Res., Part 2, Top. Stud. Oceanogr. 54, 687–705. https://doi.org/10.1016/j.dsr2.2007.01.007.

Paytan, A., Kastner, M., 1996. Benthic Ba fluxes in the central equatorial Pacific, implications for the oceanic Ba cycle. Earth Planet. Sci. Lett. 142, 439–450.

Paytan, A., Kastner, M., Martin, E.E., Macdougall, J.D., Herbert, T., 1993. Marine barite as a recorder of strontium isotopes. Nature 366, 445–449.

Paytan, A., Martinez-Ruiz, F., Eagle, M., Ivy, A., Wankel, S.D., 2004. Using sulfur isotopes to elucidate the origin of barite associated with high organic matter accumulation events in marine sediments. Spec. Pap., Geol. Soc. Am. 379, 151–160. https://doi.org/10.1130/0-8137-2379-5.151.

Paytan, A., Mearon, S., Cobb, K., Kastner, M., 2002. Origin of marine barite deposits: Sr and S isotope characterization. Geology 30, 747–750.

Polyakov, V.B., Kharlashina, N.N., 1994. Effect of pressure on equilibrium isotopic fractionation. Geochim. Cosmochim. Acta 58, 4739–4750.

Rooze, J., Peterson, L., Peterson, R.N., Meile, C., 2020. Porewater flow patterns in surficial cold seep sediments inferred from conservative tracer profiles and early diagenetic modeling. Chem. Geol. 536. https://doi.org/10.1016/j.chemgeo.2020.119468.

Rushdi, A.I., Mcmanus, J., Collier, R.W., 2000. Marine barite and celestite saturation in seawater. Mar. Chem. 69, 19–31.

Rutsch, H.-J., Mangini, A., Bonani, G., Dittrich-Hannen, B., Kubik', P.W., Suter, M., Segl, M., 1995. 10Be and Ba concentrations in West African sediments trace productivity in the past. Earth Planet. Sci. Lett. 133, 129–143.

Saunders, J.K., McIlvin, M.R., Dupont, C.L., Kaul, D., Moran, D.M., Horner, T., Laperriere, S.M., Webb, E.A., Bosak, T., Santoro, A.E., Saito, M.A., 2022. Microbial functional diversity across biogeochemical provinces in the central Pacific Ocean. Proc. Natl. Acad. Sci. 119. https://doi.org/10.1073/pnas.2200014119.

Siebert, Christopher, Nägler, Thomas F., Kramers, Jan D., 2001. Determination of molybdenum isotope fractionation by double-spike multicollector inductively coupled plasma mass spectrometry. Geochem. Geophys. Geosyst. 2.

Snelgrove, S.H., Forster, C.B., 1996. Impact of seafloor sediment permability and thickness on off-axis hydrothermal circulation: Juan de Fuca Ridge eastern flank. J. Geophys. Res. B, Solid Earth 101, 2915–2925. https://doi.org/10.1029/95jb03115.

Tang, J., Niedermayr, A., Köhler, S.J., Böhm, F., Kisakürek, B., Eisenhauer, A., Dietzel, M., 2012. Sr 2+/Ca 2+ and 44Ca/40Ca fractionation during inorganic calcite formation: III. Impact of salinity/ionic strength. Geochim. Cosmochim. Acta 77, 432–443. https://doi.org/10.1016/j.gca.2011.10.039.

Torapava, N., Ramebäck, H., Curti, E., Lagerkvist, P., Ekberg, C., 2014. Recrystallization of 223Ra with barium sulfate. J. Radioanal. Nucl. Chem. 301, 545–553. https://doi.org/10.1007/s10967-014-3170-6.

Turchyn, A.v., Schrag, D.P., 2006. Cenozoic evolution of the sulfur cycle: insight from oxygen isotopes in marine sulfate. Earth Planet. Sci. Lett. 241, 763–779. https://doi.org/10.1016/j.epsl.2005.11.007.

Turchyn, A.V., Schrag, D.P., 2004. Science 303, 2004–2007.

van Zuilen, K., Müller, T., Nägler, T.F., Dietzel, M., Küsters, T., 2016. Experimental determination of barium isotope fractionation during diffusion and adsorption processes at low temperatures. Geochim. Cosmochim. Acta 186, 226–241. https://doi.org/10.1016/j.gca.2016.04.049.

Vinograd, V.L., Brandt, F., Rozov, K., Klinkenberg, M., Refson, K., Winkler, B., Bosbach, D., 2013. Solid-aqueous equilibrium in the BaSO4-RaSO4-H2O system: first-principles calculations and a thermodynamic assessment. Geochim. Cosmochim. Acta 122, 398–417. https://doi.org/10.1016/j.gca.2013.08.028.

Vital, M., Daval, D., Morvan, G., Martinez, D.E., Heap, M.J., 2020. Barite growth rates as a function of crystallographic orientation, temperature, and solution saturation state. Cryst. Growth Des. 20, 3663–3672. https://doi.org/10.1021/acs.cgd.9b01506.

von Allmen, K., Böttcher, M.E., Samankassou, E., Nägler, T.F., 2010. Barium isotope fractionation in the global barium cycle: first evidence from barium minerals and precipitation experiments. Chem. Geol. 277, 70–77. https://doi.org/10.1016/j.chemgeo.2010.07.011.

Wasylenki, L.E., Rolfe, B.A., Weeks, C.L., Spiro, T.G., Anbar, A.D., 2008. Experimental investigation of the effects of temperature and ionic strength on Mo isotope fractionation during adsorption to manganese oxides. Geochim. Cosmochim. Acta 72, 5997–6005. https://doi.org/10.1016/j.gca.2008.08.027.

Wetzel, F., de Souza, G.F., Reynolds, B.C., 2014. What controls silicon isotope fractionation during dissolution of diatom opal? Geochim. Cosmochim. Acta 131, 128–137. https://doi.org/10.1016/j.gca.2014.01.028.

Wiederhold, J.G., Kraemer, S.M., Teutsch, N., Borer, P.M., Halliday, A.N., Kretzschmar, R., 2006. Iron isotope fractionation during proton-promoted, ligand-controlled, and reductive dissolution of goethite. Environ. Sci. Technol. 40, 3787–3793. https://doi.org/10.1021/es052228y.

Yao, W., Griffith, E., Paytan, A., 2021. Pelagic Barite: Pelagic Barite: Tracer of Ocean Productivity and a Recorder of Isotopic Compositions of Seawater S, O, Sr, Ca and Ba, Pelagic Barite. Cambridge University Press.

Yu, Y., Hathorne, E., Siebert, C., Felis, T., Rajendran, C.P., Frank, M., 2022. Monthly resolved coral barium isotopes record increased riverine inputs during the South Asian summer monsoon. Geochim. Cosmochim. Acta 329, 152–167.

Zhang, F., Frýda, J., Fakhraee, M., Lin, Y. bo, Wei, G.Y., Cao, M., Li, N., Zhou, J., Frýdová, B., Wei, H., Shen, S. zhong, 2022. Marine anoxia as a trigger for the largest Phanerozoic positive carbon isotope excursion: evidence from carbonate barium isotope record. Earth Planet. Sci. Lett. 584. https://doi.org/10.1016/j.epsl.2022.117421.

Zhen-Wu, B.Y., Dideriksen, K., Olsson, J., Raahauge, P.J., Stipp, S.L.S., Oelkers, E.H., 2016. Experimental determination of barite dissolution and precipitation rates as a function of temperature and aqueous fluid composition. Geochim. Cosmochim. Acta 194, 193–210. https://doi.org/10.1016/j.gca.2016.08.041.